Formation of synthetic RNA protein granules using engineered phage-coat-protein -RNA complexes

Naor Granik
Technion – Israel Institute of Technology
Noa Katz
Technion
Or Willinger
Technion - Israel Institute of Technology
Sarah Goldberg
Technion – Israel Institute of Technology
Roee Amit (roeeamit@technion.ac.il)
Technion - Israel Institute of Technology https://orcid.org/0000-0003-0580-7076

Article

Keywords:

Posted Date: April 20th, 2022

DOI: https://doi.org/10.21203/rs.3.rs-1546005/v1

Version of Record: A version of this preprint was published at Nature Communications on November 10th, 2022. See the published version at https://doi.org/10.1038/s41467-022-34644-4.

Abstract

Liquid-solid transition, also known as gelation, is a specific form of phase separation in which the interacting molecules cross-link to form a highly interconnected compartment with solid – like dynamical properties. Here, we utilize RNA hairpin coat-protein binding sites to form synthetic RNA based gel-like granules via liquid-solid phase transition. we show both *in-vitro* and *in-vivo* that hairpin containing synthetic long non-coding RNA (slncRNA) molecules granulate into bright localized puncta. We further demonstrate that upon introduction of the coat-proteins, less-condensed gel-like granules form with the RNA creating an outer shell with the proteins mostly present inside the granule. Moreover, by tracking puncta fluorescence signals over time, we detected addition or shedding events of slncRNA-CP nucleoprotein complexes. Consequently, our granules constitute a genetically encoded storage compartment for protein and RNA with a programmable controlled release profile that is determined by the number of hairpins encoded into the RNA. Our findings have important implications for both the potential regulatory role that naturally occurring granules play and for the broader biotechnology and gene-expression sectors.

Introduction

Phase separation, the process by which a homogeneous solution separates into multiple distinct phases, has been connected to a wide range of natural cellular processes in virtually all forms of life[1–5]. In cells, phase separation results in the formation of membrane-less compartments containing a high-concentration mix of biomolecules (e.g., proteins, RNA, etc.), which are surrounded by a low-concentration solution. Generally, phase separations are classified by the different material states which can lead to multiple types of transitions (e.g., liquid-solid, gas-liquid, etc.). The forms commonly reported in cellular biology are broadly liquid-liquid and liquid-solid (e.g., gelation), however determining the exact mechanisms for phase separation in a living cellular environment is often challenging[5].

Liquid-liquid phase transitions can be distinguished from liquid-solid by the dynamical properties of the resulting condensates. Liquid-based condensates show rapid internal rearrangement of molecules, fusions between different condensates upon contact, and dependency on the concentration of the molecules in the condensed phase[6,7]. On the other hand, liquid-solid based condensates show none of the above qualities and are mainly dependent on the number of ‘cross-linkers’, which are points of contact between the molecules, rather than on the concentration of the molecules themselves[8–10].

Recently, Jain & Vale[11] reported on the formation of RNA granules both *in vivo* and *in vitro*, from highly repetitive RNA sequences associated with repeat expansion diseases. These RNA sequences, comprised of dozens of triplet-repeats of CAG or CUG nucleobases, form intramolecular hairpin structures[12], which facilitate multivalent intermolecular interactions. The RNA granules presented features associated with liquid-solid phase transition systems: a lack of internal mobility, virtually no fusion events, and dependence on the number of repeats in the RNA sequence (i.e., cross linkers) rather than the concentration of the RNA. These characteristics helped establish the granules as physical solids.

Hairpin forming RNA sequences are widespread in the RNA world and are not strictly associated with disease phenotypes. Such sequences are commonly used in synthetic systems for biological research. Perhaps the most ubiquitous system is composed of RNA sequences that encode for multiple hairpin motifs that can bind the phage coat proteins (CPs) of PP7 or MS2. Using this system to label the 5' or 3' end of a transcript has become commonplace in the last two decades[13–18], and enables visualization of RNA transcripts when the CPs are co-expressed. This approach, originally introduced by Singer and others[13–15], was devised for the purpose of probing the dynamics of transcription and other RNA-related processes, irrespective of cell-type. When co-expressed, the coat-protein-bound RNA molecules yield bright puncta, which are similar in appearance to natural biomolecular condensates. Consequently, we hypothesized that co-suspension of synthetic RNA hairpin cassettes together with their binding CPs can lead to the formation of gel-like particles via liquid-solid phase separation *in vitro*. In addition, by utilizing the CP binding ability of the hairpins, we expect to be able to selectively incorporate proteins of our choosing into the solid-like granules, resulting in a selective platform for the stable concentration of proteins.

In this paper, we rely on our previous works[19–21] to design and synthesize a variety of PP7 coat-protein (PCP) binding synthetic long non-coding RNA molecules (slncRNAs). Using fluorescent RNA nucleotides, we show that these slncRNAs form isolated puncta *in vitro* in a manner dependent on the number of hairpins encoded into the RNA. We further show that addition of fluorescent PCP to the suspension results in almost complete co-localization between protein and slncRNA. By tracking puncta fluorescence signals over time, we demonstrate that for all slncRNAs used, the various puncta emitted similar signals characterized by bursts of increasing or decreasing fluorescent intensity. We further show that signal intensities and temporal characteristics are dependent on the number of hairpins present in the RNA. Using these observations, we conclude that these "fluorescence-bursts" corresponded to addition or shedding of slncRNA-PCP nucleoprotein complexes. These events occur at rates that are consistent with the puncta being phase-separated solid-like granules. Consequently, we present these slncRNA-protein granules as a genetically encoded platform for the selective storage of proteins as well as a model system for exploration of liquid-solid phase separation.

Results

Hairpin containing RNA phase separates *in vitro* into gel-like granules

To test whether hairpin containing RNA can phase separate *in vitro* we designed six synthetic long non-coding RNA (slncRNA) binding-site cassettes using our binding site resource[19–21]. We divided our slncRNAs into two groups. For the first group (class I slncRNAs), we designed three cassettes consisting of three, four, or eight hairpins that encode for PCP binding sites (PCP-3x, PCP-4x, and PCP-8x, respectively). In this group, hairpins were spaced by a randomized sequence that did not encode for a particular structure. For the second group (class II slncRNAs), we encoded three cassettes that consisted of three, four, and fourteen PCP binding that were each spaced by hairpin structures that do not bind PCP (PCP-3x/MCP-3x, PCP-4x/MCP-4x, and PCP-14x/MCP-15x, respectively). The sequences encoding for the

slncRNAs were cloned downstream to a pT7 promoter and transcribed *in vitro* to generate the corresponding RNA. To visualize the RNA, we incorporated fluorescent nucleotides in the transcription reaction such that an estimated 30% of uracil bases were tagged by Atto-488 fluorescent dye. Each slncRNA-type was separately mixed with granule forming buffer (see methods and Figure. 1a) at equal concentration (8.5 nM final concentration) and incubated for 1 hour at room temperature. 2 µl of the granule reaction were then deposited on a glass slide and imaged using an epi-fluorescent microscope.

The images show formation of a multitude of bright localized fluorescent condensates for all slncRNA types except for the PCP-3x case, where no such structures were detected (Figure 1b). In addition, the longer slncRNA molecules (e.g., PCP-8x and PCP-14x/MCP-15x) also exhibit larger structures, consistent with a gel like solid network, in addition to the smaller condensates or puncta. An examination of the median fluorescence obtained for each slncRNA type condensate (Figure 1c) reveals a dependence on the number of fluorescently labelled uracil nucleotides or the number of hairpins encoded into the slncRNA. However, the relationship between the median fluorescence values obtained for each species is not consistent with a linear dependence on hairpins, and instead suggests a more complex set of structures.

To further analyze the condensate structure, we fitted the measured condensate fluorescence intensity distributions to a modified Poisson distribution (see Figure 1d, Figure S1 and Supplementary methods). The panels reveal three characteristic distributions. For PCP-4x, an exponential distribution is recorded (i.e., λ=0). For PCP-3x/MCP-3x, PCP-4x/MCP-4x, and PCP-8x, a Poisson distribution of λ~1-2 seems to be the best fit. Finally, for the PCP-14x/MCP-15x, a Poisson distribution of λ~3-5 fit best. These results are consistent with the formation of condensates that are characterized by an increasing number of slncRNA molecules that are cross-linked to form a gel-like "granule", where the number of hairpins encoded into the slncRNA determines the average number of molecules or cross-links within the observed field of granules. Moreover, the interpretation suggested by the shape of the distribution is contrasted by the counter-intuitive observation of decreasing value of the of the fitting parameter K_0 as a function of an increasing number of hairpins (Figure 1e). In this particular context, this observation is manifested by a significantly more gradual increase in mean or median granule fluorescence as compared to what would be naively expected by a simple rescale that takes into account the number of hairpins. Together, these observations suggest that slncRNA granules form via cross-linking interaction of multiple slncRNA molecules, and that an increasing number of hairpins and cross-links lead to a denser condensate. Denser granules, in turn, may result in fluorescence quenching of the labelled uracils[22] leading only to a gradual and disproportionate increase in fluorescence observed.

RNA-based granules co-localize with protein-binding partners

To test if the hairpins retain their ability to bind the PP7 phage coat protein while in the granule state, we added recombinant tandem dimer PP7 coat protein fused to mCherry (tdPCP-mCherry) to the granule formation reaction in excess amount (final concentration 25 nM) to account for the multiple binding sites present on one slncRNA molecule (Figure 2a). The tdPCP-mCherry version used lacks the

necessary moiety to form the wildtype viral capsid[23]. The images (Figure 2b) show colocalization between the 488 nm channel (Atto-488) and the 585 nm channel (mCherry) for all slncRNA designs used in the experiment implying that PP7 coat proteins are able to bind the RNA hairpins in the condensate state. Hence, the slncRNA and their protein partners form synthetic RNA-protein (SRNP) granules. Unexpectedly, PP7-3x granules were witnessed in the presence of the protein, implying that tdPCP-mCherry adds a measure of multivalency to the system, and thus triggers condensation of RNA molecules that do not phase separate on their own. To check that this condensation was hairpin dependent, we tested whether a control RNA (of the same length and GC content as PCP-8x) containing no designed hairpin condensed either on its own or in the presence of tdPCP-mCherry forms granules. In both cases, no condensates were detected in either the 488 nm or 585 nm channels (data not shown). Finally, unlike for the slncRNA only case, SRNP granules (particularly for high number of hairpins) show an increased propensity to form large-scale extended structures, suggesting a more complex structure formation and condensation for the SRNP granules as compared with the slncRNA-only case.

Next, we measured the median fluorescence intensity of the mCherry protein in different SRNP granules. The distributions of median values (Figure 2c) show a clear dependence on the number of binding sites available for protein binding. First, the PCP-3x/MCP-3x and PCP-4x granules appear to have a similar number of proteins in the granule and are both weaker than PCP-4x/MCP-4x granules, suggesting that PCP-4x slncRNAs inside the granules are not fully occupied by proteins. In addition, the PCP-14x/MCP-15x granules seems to be >2-fold brighter as compared with the PCP-8x granules, despite having <2-fold the number of hairpins. This stands in contrast to the observation that PCP-14x/MCP-15x granules appear to be ~3 times brighter than PCP-4x/MCP-4x granules, reflecting the difference in the number of binding sites available for binding. Finally, PCP-3x granules appear to be half as bright as PCP-14x/MCP-15x granules, providing more evidence that the former are not RNA-dependent entities. We also observe that when the spacing regions within the slncRNA encode for the MCP hairpins, the formed granules contain a larger protein cargo.

To confirm this observation, we also observed the SRNP granules in the 488 nm channel. Here a similar image emerges, whereby the median fluorescence values for each granule are percentage-wise more differentiated as compared with the slncRNA-only case, reflecting a more proportional increase in fluorescence (Figure. 2d). Together, the observations in both channels indicate that SRNP granules are less dense gel-like structures as compared with the slncRNA-only granules. To authenticate the granules as being solid-like RNA-protein structures, we imaged them using a SIM super resolution microscope with 120 nm resolution. Figure 2e shows a sample image of a PCP-14x/MCP-15x granule containing the tdPCP-mCherry protein. The image shows that slncRNA is found mainly in the periphery of the granule, with filaments protruding into its core, where a high amount of protein is amassed in a network like configuration. The RNA seems to encase the protein cargo in a reduced density structure.

Finally, we explored the phase space of SRNP granule formation. To do so, we characterized formation of the PCP-14x/MCP-15x SRNP granules as a function of both slncRNA and protein concentration. For this we produced non-fluorescent RNA molecules (for higher concentrations) and mixed different titers of

slncRNA and tdPCP-mCherry protein, each varied over two orders of magnitude. Puncta like structures were detected only for slncRNA and proteins concentrations of 100 ng/μl and above (Figure. 2f). The images display bright puncta that are embedded within a filamentous structure. Quantification of the maximal intensity of the puncta both at time T=0 (i.e., beginning of the reaction) and time T=1 [hr] (Figure. 2g) reveals a fluorescent intensity distribution which declines by two orders of magnitude (i.e., from ~10^5 to ~10^3) in a step-like function as the RNA concentration is reduced from 1000 to 10 ng/μl, providing further indication that RNA is essential for granule formation. Likewise, the intensity distribution of the puncta declines in a more gradual fashion as the protein concentration is reduced, but overall, a similar disappearance of puncta is observed.

Temporal tracking of individual SRNP granules reveals that granules function as protein capacitors

A hallmark of phase separation is the exchange of molecules between the dilute phase and the dense phase. This is also true for gels with non-permanent intermolecular interactions, wherein random breaks and rearrangement of the connections which form the inner network allow macromolecules (monomers and small polymers) to diffuse in and out of the gel phase[8–11], albeit at a slow rate. These exchange events are predicted to occur independently of one another, at a rate which depends on multiple parameters: the probability of cross linking within the gel network (i.e., number of hairpins), the transient concentration of the molecules in the surrounding solution, and the average diffusion rate of the monomers. The movement of molecules (fluorescent CPs, slncRNA, and CP-bound slncRNA complexes) between the different phases should be reflected by changes in granule fluorescence intensity.

To test whether the synthetic granules display this characteristic, we tracked the fluorescence intensity of each granule in a given field-of-view for 60 minutes. We analyzed the brightness of each granule at every time point using a customized analysis algorithm (see Supplementary Methods). The resulting signals are either decreasing or increasing in overall intensity, and dispersed within them are sharp variations in brightness, that are also either increasing or decreasing. Next, we employed a statistical threshold which flagged these signal variation events, or “signal bursts”, whose amplitude was determined to not be part of the underlying signal distribution (p-value<1e-3) (See Supplementary Methods for definitions of bursts, algorithm details, and relevant numerical controls). The events were classified as either increasing bursts (green), decreasing bursts (red), or non-classified segments (blue), which are segments where molecular movement cannot be discerned from the noise (Figure. 3a). For each detected burst, we measure its amplitude (Δ intensity) and duration (Δ time), in addition to measuring the time between bursts and the order of their appearance. In Figure. 3b we plot the distributions of amplitudes for all three event types, obtained from ~156 signal traces, each gathered from a different granule composed of PCP-14x/MCP-15x and tdPCP-mCherry. We observe a bias towards negative burst or shedding events. Assuming an interpretation that fluorescent burst events correspond to insertion and shedding events of slncRNA-CP complexes into or out of the synthetic granules, the amplitude bias towards negative events is consistent with RNA degradation and lack of transcription within the *in vitro* suspension, leading to a net shedding of slncRNA molecules out of the granules over time.

We repeated the tracking process for granules produced from all previously-described slncRNA designs (including the PP7-3x which does not phase separate on its own). Comparison of the amplitude distributions per design (class I vs. II), (Figure. 3c) reveals a dependence on the number of hairpins available for protein binding, where more protein binding sites translate directly into larger amplitudes. Next, we also measured burst amplitude in the green-channel to confirm that bursts indeed correspond to the shedding of a slncRNA-protein complex from the granule. Figure. 3d shows a sample signal for the PCP-14x/MCP-15x granules showing concomitant occurrence of bursts in both the red and green channels, supporting our interpretation of this signal. Using the burst distributions, we then computed the ratio between the mean granule fluorescence and the mean burst amplitude, providing a measure for the number of slncRNA molecules within the granule. The results (Figure. 3e-f) show that with the exception of the PCP-4x based SRNP granules, the ratio in the green channel is 5, suggesting that a typical granule contains five slncRNAs. The ratio computed for the red channel is typically smaller, and for PCP-8x is ~2. This means that in every burst approximately half the protein content is released with the RNA. This further implies that PCP-8x may be permeable to proteins diffusing out of the granules due to reduced cross-linking as a result of a lack of hairpin spacing structures. For the PCP-3x/MCP-3x, PCP-4x/MCP-4x, and PCP-14x/MCP-15x the ratio in the red channel is approximately equal to that of the green channel, suggesting that these granules have a better protein storage capacity. Hence, the granules composed of class II slncRNA seem to form more robust and better insulated granules from the perspective of their protein storage capacity.

To provide further evidence for this interpretation, we measured the time duration between events for each granule type. For the granules, this rate (~5 minutes) is two orders of magnitude above the typical rate observed in liquid phase separated condensates[24], but is in line with the measurements performed on RNA gels by Vale et. al.[11], providing additional confirmation that the SRNP granules are gel-like particles. A closer examination of the duration boxplots (Figure. 3g) obtained for each granule-type reveals that more binding sites lead to longer durations on average, for both negative and positive bursts. Additionally, there appears to be a difference between the slncRNA designs themselves. While the granules composed of class I slncRNA granules present on average longer durations between positive bursts, compared to negative bursts, the opposite is true for the class II slncRNAs. Assuming a roughly uniform distribution of molecules outside of the granule (given enough time to equilibrate), this may mean that on average, a protein-bound slncRNA molecule has a higher probability of leaving a class I slncRNA granule than entering it, and vice versa for the class II slncRNA granules. This result confirms the interpretation of the burst ratio analysis, and together these results imply that class II granules are characterized by a highly-cross-linked slncRNA network which prevents the diffusion away of molecules (leading to a longer time between negative bursts), while the granule boundary still contains free cross-linking points that can latch on to incoming molecules more easily, increasing the chances of molecular entry (leading to a shorter time between positive bursts). Together, these SRNP granule characteristics are reminiscent of data and energy storage devices (e.g., capacitors), with the protein cargo replacing the electric charge in the biochemical analog.

Expression of slncRNAs and protein in bacteria yields puncta-like condensates

Given the capacitor analogy, we hypothesized that *in vivo* the granules can be used as devices that store the granule-bound proteins. This is due to the steady state production of slncRNAs and proteins via the cellular transcriptional and translational machinery, that ensures a constant flux of proteins into the granules. To show this, we first proceeded to test whether the granule material characteristics that are measured *in vivo* match the *in vitro* measurements. To do so, we decided to utilize two previously reported slncRNA designs which were shown to yield bright localized puncta *in vivo* in earlier work[19]. The first slncRNA is of a class II design, PCP-4x/ QCP-5x, consisting of four native PCP binding sites and five native Qβ coat protein (QCP) hairpins used as spacers in an interlaced manner. The second slncRNA is the ubiquitous PCP-24x cassette[25], which from the perspective of this work can be regarded as a class I design slncRNA.

To confirm the granules form conditions *in vivo*, we encoded the slncRNA component under the control of a T7 promoter, and the tdPP7-mCherry under the control of an inducible pRhlR promoter (Figure. 4a). We first wanted to test whether puncta develop *in vivo* and whether they are dependent on the existence of hairpins in the RNA. For this we co-transformed plasmids encoding either the negative control RNA or the PCP-4x/QCP-5x slncRNA, together with a plasmid encoding for the tdPCP-mCherry protein, into BL21-DE3 *E. coli* cells. Examination of cells expressing the slncRNA and protein following overnight induction of all components revealed the formation of bright puncta at the cell poles (Figure. 4b), which were absent in cells expressing the control RNA which lacks hairpins (Figure. 4c).

Next, to test whether cellular concentration of slncRNA influences the formation of the granules, we quantified the fraction of puncta per cell for cells expressing the PCP-4x/QCP-5x from a multicopy expression vector, and cells expressing the same slncRNA from a bacterial artificial chromosome (BAC) expression vector which is maintained at a single copy level in cells. We found that cells containing the multicopy plasmid frequently present puncta in at least one of the poles, while cells containing the single copy generally show between zero and one punctum (Figure. 4d). Given that cells expressing the slncRNAs from single copy vectors still present puncta, we decided to continue using this expression vector in follow-up experiments to reduce variability stemming from copy number differences.

We compared cells expressing the PCP-4x/ QCP-5x or the PCP-24x (expressed from a BAC vector) in terms of the spot per cell fraction. Much like in the *in vitro* experiments, we found a dependence on the number of binding sites in accordance with the *in vitro* results and the cross linking model of gel phase formation[6,26] (Figure. 4d). Finally, to test whether the polar localization of the granules is a consequence of nucleoid exclusion[27], we grew the cells in starvation conditions for several hours, triggering a transition to stationary phase. In stationary phase the nucleoid is known to condense[28–30], thus increasing the amount of cellular volume which is likely to be molecularly dilute. This, in turn, generates a larger accessible cellular volume for granule formation, which should lead to different presentation of the phase-separation phenomena as compared with exponentially growing cells. In Figure. 4e, we show images of bacteria displaying ‘bridging’ (the formation of a high intensity streak between the spots) of

puncta (left), whereby granules seem to fill out the available dilute volume, and the emergence of a third puncta at the center of the cell (right). Both behaviors are substantially different than the puncta appearing under normal conditions. Such behavior was observed in >40% of the fluorescent cells and was not detected in non-stationary growth conditions. Thus, SRNP granules with characteristics that are consistent with the *in vitro* observations form *in vivo*, in a semi-dilute bacterial cytosolic environment and independent of cell-state.

slncRNA expression increases cellular protein concentration

To investigate the dynamic properties of granules formed *in vivo*, we utilized the same analysis approach as was used in the *in vitro* experiments, with minor differences. Normalizing the fluorescence of the granule by that of the cell (see methods) for every time point results in a signal vs. time trace largely independent from the effects of photobleaching and cellular background noise, allowing us to search for and measure burst events, as was done previously. In Figure. 5a, we plot the distributions of amplitude (Δ intensity) of all three event types (positive, negative, and non-classified), obtained from 255 traces gathered from cells expressing the PCP-4x/QCP-5x slncRNA together with the tdPCP-mCherry protein. The symmetry in both shape and spread of the negative and positive distributions indicates that both are measurements of the same type of macromolecule, distinguished only by the direction in which it travels (into or out of the granule). Moreover, a similarly symmetric burst distribution is recorded for the PCP-24x slncRNA (Figure S1). This result contrasts with the *in vitro* amplitude distribution data (Figure 3b), which presented a skewness towards negative bursts. This implies that *in vivo,* the transcriptional and translational processes in the cell balance the loss of granule components due to degradation.

Next, we measured the amplitudes of the bursts for both slncRNAs and found that positive and negative amplitudes are proportional to the number of binding sites within the encoded cassette (Figure 5b). In addition, a more quantitative analysis of these distributions (Figure S2) reveals that a single burst for the 24x cassette is ~2.5-3x more fluorescent as compared with the 4x cassette, indicating that the molecules transitioning in and out of the 24x granules are slncRNAs partially or fully bound rather than lone proteins. Moreover, estimations of the positive and negative amplitudes are practically equal per slncRNA, providing additional evidence that these are in fact representations of one physical process, with the difference being the directionality of the transitioning slncRNA-protein molecule. Finally, we measured the duration between burst events, revealing that slow shedding and absorption processes on the order of minutes are taking place for the *in vivo* granules as well (Figure 5c). Altogether, the non-existence of puncta in cells expressing the negative control RNA, the slow exit/entry rate of molecules, and the dependence on the number of binding sites, suggest that synthetic RNA protein granules are phase separated condensates *in vivo* and possess the same gel-like characteristics that were observed for the *in vitro* suspensions. Consequently, *in vivo* burst analysis is consistent with the capacitor model, where the amount of protein stored within the SRNP granule seems to be in steady state when there is a steady supply of protein and slncRNA.

Next, to ascertain whether the granules facilitate increased protein titers *in vivo* in accordance with the capacitor model predictions, we measured for each bright granule the mean fluorescence intensity (Figure 5d), and the mean intensity of the cell which contains it (Figure 5e). We observed a dramatic increase in mean cellular fluorescence between cells which express only tdPCP-mCherry and cells which express it together with a slncRNA, suggesting that slncRNA molecules have some effect in the cytosol, regardless of the granules. To quantify this phenomenon more accurately, we measured the total fluorescence of the population using flow cytometry. For this, we grew cells expressing only the protein component (tdPCP-mCherry), and cells expressing both protein and a slncRNA (PCP-4x/QCP-5x or PCP-24x), with different combinations of induction: IPTG (induces the slncRNA) and C4HSL (induces the protein). The data (Figure 5f) shows that cells expressing a slncRNA, regardless of induction (due to T7 leakiness), show higher fluorescence than cells expressing the protein only. In addition, induction of slncRNA expression with IPTG results in an increase in fluorescence, indicating that slncRNA is a deciding factor in this behavior. Finally, cells expressing the PCP-24x slncRNA show higher fluorescence than cells expressing PCP-4x/QCP-5x, displaying a dependence of the cellular protein titer on number of binding sites available for protein binding.

Discussion

In this study, we show that synthetic gel-like RNA – protein granules can be designed and assembled using phage coat proteins and RNA molecules that encode multiple CP binding sites, both in suspension and *in vivo*. Using fluorescently labelled RNA, we show that granule formation is nucleated by RNA-RNA interactions that are proportional to the number of hairpins encoded into the RNA. In addition, the binding of the proteins seems to further enhance and assist the granule formation process. Using fluorescent single molecule signal analysis, we reveal entry and exit events of molecules into and out of the granules. By investigating their size and rate of occurrence, we show that these events correspond to entry and shedding of protein-bound slncRNA molecules, and that they are dependent on the number of hairpins available for protein binding. Transitioning of macro-molecules across a phase boundary is frequently observed in phase-separated condensates, particularly in liquld-liquid based system. In particular, the frequency of these transitions reflects the underlying order, internal interactions, and density of the condensed phase. While in liquid-liquid phase separation systems such transitions occur on the scale of seconds or less, here we observe shedding and insertion events on a much longer time scale of minutes or longer, that is more consistent with a solid or gel-like condensed phase. The slow release and strong internal interactions which keep the granules intact for long durations, combined with the selectivity of our system due to the RNA binding component, could be utilized as a programmable controlled release mechanism in suitable biological settings. Hence, our granules can be thought as protein and RNA storage modules akin to a capacitor, with a monophasic release profile that can be tuned based on the slncRNA design.

We further characterized two options for slncRNA design: a homogeneous design which is comprised of multiple CP hairpin binding site and non-structured spacing regions (class I), and a hybrid design which is comprised of hairpin binding sites and additional hairpins in the spacing regions (class II). We show that

the design choice has implications for the granule's protein-carrying capacity and dynamics. In particular, class II granules formed particles with increased cross-linking capability in the RNA-only granule, which in turn led to an increased ability to insulate the protein cargo in the SRNP granule phase. On the flip side, class I granules were characterized by decreased cross-linking in the RNA-only phase and increased permeability of the protein cargo in the SRNP-granule phase. In addition, class I granules displayed a faster shedding or dissolution rate, which in turn lead to a smaller protein cargo on average. This two-dimensional phase space of capacity vs. rigidity offers substantial flexibility and tunability when designing SRNP granules for a variety of applications.

The capacitor- or storage-like behavior displayed by the SRNP granules implies that *in vivo*, the granules together with the gene-expression machinery form a biochemical analog of an RC-circuit. In a conventional RC-circuit, energy is stored within the capacitor for release at a later time. Such circuits are often used to protect electrical devices against sudden surges or stoppages of power. Here, the protein and slncRNA flux into the cytosol correspond to the current, which results in the formation of fully "charged" SRNP granules. This genetically encoded slncRNA and protein storage facility, which is constantly maintained, effectively increases the protein and slncRNA content of the cell beyond the steady-state levels facilitated by standard transcription, translation, RNA degradation, and proteolysis. This storage capacity is precisely the function that is carried out by capacitors in RC-circuits, allowing electrical devices to function even after "power" is cut-off. In the case here, the granules can be used not only to increase levels of a protein of choice by nearly an order of magnitude (as shown in Fig. 5) without adversely affecting the cell, but may also provide a mechanism to increase the cell's ability to survive when a harsh or stressful environment is encountered. While the former may have important implications to the biotechnology sector, the latter may hint at an important function that natural granules (e.g., paraspeckles, p-bodies, etc.) may have evolved for *in vivo*. Further studies will be required to explore the biological relevance of RNP granules to the survivability of cells and organisms under various forms of stress.

Materials And Methods

Bacterial strains

E. coli BL21-DE3 cells which encode the gene for T7 RNAP downstream from an inducible pLac/Ara promoter were used for all reported experiments. *E. coli* TOP10 (Invitrogen, Life Technologies, Cergy-Pontoise) was used for cloning procedures.

Addgene plasmids

pCR4-24XPP7SL was a gift from Robert Singer (Addgene plasmid # 31864; http://n2t.net/addgene:31864; RRID: Addgene_31864).

pBAC-lacZ was a gift from Keith Joung (Addgene plasmid # 13422; http://n2t.net/addgene:13422; RRID: Addgene_13422).

Construction of the slncRNA plasmids

All sequences encoding for the *in vitro* slncRNAs (i.e., PP7-3x, PP7-4x, PP7-3x/MS2-3x, PP7-4x/MS2-4x, PP7-8x and PP7-14x/MS2-15x) were ordered from Integrated DNA Technologies (IDT) (Coralville, Iowa) as gBlock gene fragments downstream to a T7 promoter and flanked by EcoRI restriction sites on both sides. gBlocks were cloned into a high-copy plasmid containing an Ampicillin resistance gene and verified using Sanger sequencing.

The 5Qβ/4PP7 slncRNA sequence was ordered from GenScript, Inc. (Piscataway, NJ), as part of a puc57 plasmid, flanked by EcoRI and HindIII restriction sites. pBAC-lacZ backbone plasmid was obtained from Addgene (plasmid #13422). Both insert and vector were digested using EcoRI and HindIII (New England Biolabs [NEB], Ipswich, MA)and ligated to form a circular plasmid. Sequence was verified by sanger sequencing.

Design and construction of fusion-RBP plasmids

Fusion-RBP plasmids were constructed as previously reported[21]. Briefly, RBP sequences lacking a stop codon were amplified via PCR off either Addgene or custom-ordered templates. Both RBPs presented (PCP and QCP) were cloned into the RBP plasmid between restriction sites KpnI and AgeI, immediately upstream of an mCherry gene lacking a start codon, under the so-called RhlR promoter containing the rhlAB las box[31] and induced by N-butyryl-L-homoserine lactone (C4-HSL) (Cayman Chemicals, Ann Arbor, Michigan). The backbone contained either an Ampicillin (Amp) or Kanamycin (Kan) resistance gene, depending on experiment.

In vitro transcription of slncRNA

A vector containing the slncRNA DNA sequence, flanked by two EcoRI restriction sites, was digested with EcoRI-HF (NEB, #R3101S) per the manufacturer's instructions to form a linear fragment encoding the slncRNA sequence. The enzyme was then heat-inactivated by incubating the restriction reaction at 65 C for 20 minutes. For fluorescently labelled RNA, 1 µg of the restriction product was used as template for in vitro transcription using HighYield T7 Atto488 RNA labeling kit (Jena Bioscience, Jena, Germany, RNT-101-488-S), according to the manufacturer's instructions. Non-fluorescent RNA was transcribed using the HiScribe™ T7 High Yield RNA Synthesis Kit (NEB, #E2040S). Following in vitro transcription by either kit, the reaction was diluted to 90 µl and was supplemented with 10 µl DNAse I buffer and 2 µl DNAse I enzyme (NEB #M0303S) and incubated for 15 minutes at 37 C to degrade the DNA template. RNA products were purified using Monarch RNA Cleanup Kit (NEB, #T2040S) and stored in -80 .

Protein expression and purification

E. coli cells expressing tdPP7-mCherry fusion protein were grown overnight in 10 ml LB with appropriate antibiotics at 37 C with 250 rpm shaking. Following overnight growth cultures were diluted 1/100 into two vials of 500 ml Terrific Broth (TB: 24 g yeast extract, 20 g tryptone, 4 ml glycerol in 1 L of water, autoclaved, and supplemented with 17 mM KH2PO4 and 72 mM K2HPO4), with appropriate antibiotics

and induction (100 µl C4-HSL) and grown in 37 C and 250 rpm shaking to OD600 > 10. Cells were harvested, resuspended in 30 ml resuspension buffer (50 mM Tris-HCl pH 7.0, 100 mM NaCl and 0.02% NaN3), disrupted by four passages through an EmulsiFlex-C3 homogenizer (Avestin Inc., Ottawa, Canada), and centrifuged (13,300 RPM for 30 min) to obtain a soluble extract. Fusion protein was purified using HisLink Protein purification resin (Promega) according to the manufacturer's instructions. Buffer was changed to 1xPBS using multiple washes on Amicon columns (Biorad).

In vitro granule microscopy

In vitro experiments were performed in granule buffer (750 mM NaCl, 1 mM MgCl2, 10% PEG4000). Reactions were set up as follows: 8 µl granule buffer, 1 µl protein, 1 µl RNA and allowed to rest at room temperature for 1 hour. 1–2 µl from the reaction was then deposited on a glass slide and imaged in a Nikon Eclipse Ti-E epifluorescent microscope (Nikon, Japan). Excitation was performed at 488 nm (Atto 488) for experiments containing fluorescent RNA, and 585 nm (mCherry) wavelengths by a CooLED (Andover, UK) PE excitation system. Images were captured using the Andor iXon Ultra EMCCD camera with a 500 msec exposure time for 488 nm and 250 msec exposure time for 585 nm.

In vivo microscopy

BL21-DE3 cells expressing the two plasmid system (single copy plasmid containing the binding sites array, and a multicopy plasmid containing the fluorescent protein fused to an RNA binding protein) were grown overnight in 5 ml Luria Broth (LB), at 37 with appropriate antibiotics (Cm, Amp), and in the presence of two inducers – 1.6 µl Isopropyl β-D-1-thiogalactopyranoside (IPTG) (final concentration 1 mM), and 2.5 µl C4-HSL (final concentration 60 µM) to induce expression of T7 RNA polymerase and the RBP-FP, respectively. Overnight culture was diluted 1:50 into 3 ml semi-poor medium consisting of 95% bioassay buffer (BA: for 1 L—0.5 g Tryptone [Bacto], 0.3 ml glycerol, 5.8 g NaCl, 50 ml 1 M MgSO4, 1 ml 10×PBS buffer pH 7.4, 950 ml DDW) and 5% LB with appropriate antibiotics and induced with 1 µl IPTG (final concentration 1 mM) and 1.5 µl C4-HSL (final concentration 60 µM). For stationary phase tests, cells were diluted into 3 ml Dulbecco's phosphate-buffered saline (PBS) (Biological Industries, Israel) with similar concentrations of inducers and antibiotics. Culture was shaken for 3 hours at 37 before being applied to a gel slide [3 ml PBSx1, mixed with 0.045g SeaPlaque low melting Agarose (Lonza, Switzerland), heated for 20 seconds and allowed to cool for 25 minutes][32]. 1.5 µl cell culture was deposited on a gel slide and allowed to settle for an additional 30 minutes before imaging.

Live cell microscopy

Gel slide was kept at 37 inside an Okolab microscope incubator (Okolab, Italy). A time lapse experiment was carried out by tracking a field of view for 60 minutes on Nikon Eclipse Ti-E epifluorescent microscope (Nikon, Japan) using an Andor iXon Ultra EMCCD camera at 6 frames-per-minute with a 250 msec exposure time per frame. Excitation was performed at 585 nm (mCherry) wavelength by a CooLED (Andover, UK) PE excitation system.

Quantification of the fraction of cells presenting puncta was done by taking 10–15 snapshots of different fields of view (FOV) containing cells. The number of cells showing puncta and the total number of fluorescent cells in the FOV were counted manually.

Declarations

Acknowledgments: The authors would like to acknowledge the Technion's LS&E staff (Tal Katz-Ezov Anastasia Diviatis, and Yael Lupu-haber) for help with sequencing and super resolution imaging experiments. In addition, the authors would like to thank professor Yoav Schectman from the Department of Biomedical Engineering in the Technion for help with image and signal analysis.

Funding: This project received funding from the I-CORE Program of the Planning and Budgeting Committee and the Israel Science Foundation (Grant No. 152/11); Marie Curie Reintegration Grant No. PCIG11-GA-2012-321675; and from the European Union's Horizon 2020 Research and Innovation Programme under grant agreement 664918 (MRG-Grammar) and 851065 (CARBP).

Author contributions: NG designed the PP7-3x, PP7-3x/MS2-3x, PP7-4x, PP7-8x and PP7-4x/MS2-4x slncRNAs and carried out the microscopy experiments and analysis for all data. NK designed and synthesized the PP7-4x/Qβ-5x, and the PP7-14x_MS2-15x slncRNAs. OHW assisted with flow cytometry experiments and data analysis, SG assisted and guided the experiments and image analysis. RA supervised the study. NG and RA wrote the manuscript.

Competing interests: The authors declare no competing interests.

Data and materials availability: All datasets and original code used in this paper are available from: https://github.com/naorgk/slncRNA_Analysis. All bacterial plasmids constructed for this work are available upon request.

References

1. Banani, S. F.; Lee, H. O.; Hyman, A. A.; Rosen, M. K. Biomolecular Condensates: Organizers of Cellular Biochemistry. Nat Rev Mol Cell Biol 2017, *18* (5), 285–298. https://doi.org/10.1038/nrm.2017.7.
2. Polymenidou, M. The RNA Face of Phase Separation. Science 2018, *360* (6391), 859–860. https://doi.org/10.1126/science.aat8028.
3. Hyman, A. A.; Weber, C. A.; Jülicher, F. Liquid-Liquid Phase Separation in Biology. Annual Review of Cell and Developmental Biology 2014, *30* (1), 39–58. https://doi.org/10.1146/annurev-cellbio-100913-013325.
4. Langdon, E. M.; Gladfelter, A. S. A New Lens for RNA Localization: Liquid-Liquid Phase Separation. Annual Review of Microbiology 2018, *72* (1), 255–271. https://doi.org/10.1146/annurev-micro-090817-062814.

5. Boeynaems, S.; Alberti, S.; Fawzi, N. L.; Mittag, T.; Polymenidou, M.; Rousseau, F.; Schymkowitz, J.; Shorter, J.; Wolozin, B.; Van Den Bosch, L.; Tompa, P.; Fuxreiter, M. Protein Phase Separation: A New Phase in Cell Biology. Trends Cell Biol. 2018, *28* (6), 420–435. https://doi.org/10.1016/j.tcb.2018.02.004.
6. Klosin, A.; Oltsch, F.; Harmon, T.; Honigmann, A.; Jülicher, F.; Hyman, A. A.; Zechner, C. Phase Separation Provides a Mechanism to Reduce Noise in Cells. Science 2020, *367* (6476), 464–468. https://doi.org/10.1126/science.aav6691.
7. Feng, Z.; Chen, X.; Wu, X.; Zhang, M. Formation of Biological Condensates via Phase Separation: Characteristics, Analytical Methods, and Physiological Implications. Journal of Biological Chemistry 2019, *294* (40), 14823–14835. https://doi.org/10.1074/jbc.REV119.007895.
8. Winter, H. H.; Mours, M. Rheology of Polymers Near Liquid-Solid Transitions. In *Neutron Spin Echo Spectroscopy Viscoelasticity Rheology*; Advances in Polymer Science; Springer: Berlin, Heidelberg, 1997; pp 165–234. https://doi.org/10.1007/3-540-68449-2_3.
9. Khalil, N.; Candia, A. de; Fierro, A.; Pica Ciamarra, M.; Coniglio, A. Dynamical Arrest: Interplay of Glass and Gel Transitions. Soft Matter 2014, *10* (27), 4800–4805. https://doi.org/10.1039/C4SM00199K.
10. Jawerth, L.; Fischer-Friedrich, E.; Saha, S.; Wang, J.; Franzmann, T.; Zhang, X.; Sachweh, J.; Ruer, M.; Ijavi, M.; Saha, S.; Mahamid, J.; Hyman, A. A.; Jülicher, F. Protein Condensates as Aging Maxwell Fluids. Science 2020, *370* (6522), 1317–1323. https://doi.org/10.1126/science.aaw4951.
11. Jain, A.; Vale, R. D. RNA Phase Transitions in Repeat Expansion Disorders. Nature 2017, *546* (7657), 243–247. https://doi.org/10.1038/nature22386.
12. Krzyzosiak, W. J.; Sobczak, K.; Wojciechowska, M.; Fiszer, A.; Mykowska, A.; Kozlowski, P. Triplet Repeat RNA Structure and Its Role as Pathogenic Agent and Therapeutic Target. Nucleic Acids Research 2012, *40* (1), 11–26. https://doi.org/10.1093/nar/gkr729.
13. Bertrand, E.; Chartrand, P.; Schaefer, M.; Shenoy, S. M.; Singer, R. H.; Long, R. M. Localization of ASH1 MRNA Particles in Living Yeast. Molecular cell 1998, *2* (4), 437–445.
14. Tutucci, E.; Vera, M.; Biswas, J.; Garcia, J.; Parker, R.; Singer, R. H. An Improved MS2 System for Accurate Reporting of the MRNA Life Cycle. Nature Methods 2018, *15* (1), 81–89. https://doi.org/10.1038/nmeth.4502.
15. Larson, D. R.; Singer, R. H.; Zenklusen, D. A Single Molecule View of Gene Expression. Trends Cell Biol 2009, *19* (11), 630–637. https://doi.org/10.1016/j.tcb.2009.08.008.
16. Jones, D.; Elf, J. Bursting onto the Scene? Exploring Stochastic MRNA Production in Bacteria. Current Opinion in Microbiology 2018, *45*, 124–130. https://doi.org/10.1016/j.mib.2018.04.001.
17. Fusco, D.; Accornero, N.; Lavoie, B.; Shenoy, S. M.; Blanchard, J.-M.; Singer, R. H.; Bertrand, E. Single MRNA Molecules Demonstrate Probabilistic Movement in Living Mammalian Cells. Current Biology 2003, *13* (2), 161–167.
18. Golding, I.; Paulsson, J.; Zawilski, S. M.; Cox, E. C. Real-Time Kinetics of Gene Activity in Individual Bacteria. Cell 2005, *123* (6), 1025–1036. https://doi.org/10.1016/j.cell.2005.09.031.

19. Katz, N.; Tripto, E.; Granik, N.; Goldberg, S.; Atar, O.; Yakhini, Z.; Orenstein, Y.; Amit, R. Overcoming the Design, Build, Test (DBT) Bottleneck for Synthesis of Nonrepetitive Protein-RNA Binding Cassettes for RNA Applications. Nature Communications 2021.
20. Katz, N.; Cohen, R.; Solomon, O.; Kaufmann, B.; Atar, O.; Yakhini, Z.; Goldberg, S.; Amit, R. Synthetic 5' UTRs Can Either Up- or Downregulate Expression upon RNA-Binding Protein Binding. Cell Systems 2019, *9* (1), 93–106.e8. https://doi.org/10.1016/j.cels.2019.04.007.
21. Katz, N.; Cohen, R.; Solomon, O.; Kaufmann, B.; Atar, O.; Yakhini, Z.; Goldberg, S.; Amit, R. An in Vivo Binding Assay for RNA-Binding Proteins Based on Repression of a Reporter Gene. ACS Synth. Biol. 2018, *7* (12), 2765–2774. https://doi.org/10.1021/acssynbio.8b00378.
22. Bae, W.; Yoon, T.-Y.; Jeong, C. Direct Evaluation of Self-Quenching Behavior of Fluorophores at High Concentrations Using an Evanescent Field. PLOS ONE 2021, *16* (2), e0247326. https://doi.org/10.1371/journal.pone.0247326.
23. Chao, J. A.; Patskovsky, Y.; Almo, S. C.; Singer, R. H. Structural Basis for the Coevolution of a Viral RNA–Protein Complex. Nature Structural & Molecular Biology 2008, *15* (1), 103–105. https://doi.org/10.1038/nsmb1327.
24. Wheeler, J. R.; Matheny, T.; Jain, S.; Abrisch, R.; Parker, R. Distinct Stages in Stress Granule Assembly and Disassembly. *eLife* 2016, *5*, e18413. https://doi.org/10.7554/eLife.18413.
25. Hocine, S.; Raymond, P.; Zenklusen, D.; Chao, J. A.; Singer, R. H. Single-Molecule Analysis of Gene Expression Using Two-Color RNA Labeling in Live Yeast. Nature Methods 2013, *10* (2), 119–121. https://doi.org/10.1038/nmeth.2305.
26. Li, P.; Banjade, S.; Cheng, H.-C.; Kim, S.; Chen, B.; Guo, L.; Llaguno, M.; Hollingsworth, J. V.; King, D. S.; Banani, S. F.; Russo, P. S.; Jiang, Q.-X.; Nixon, B. T.; Rosen, M. K. Phase Transitions in the Assembly of Multivalent Signalling Proteins. Nature 2012, *483* (7389), 336–340. https://doi.org/10.1038/nature10879.
27. Neeli-Venkata, R.; Martikainen, A.; Gupta, A.; Gonçalves, N.; Fonseca, J.; Ribeiro, A. S. Robustness of the Process of Nucleoid Exclusion of Protein Aggregates in Escherichia Coli. Journal of Bacteriology *198* (6), 898–906. https://doi.org/10.1128/JB.00848-15.
28. Kim, J.; Yoshimura, S. H.; Hizume, K.; Ohniwa, R. L.; Ishihama, A.; Takeyasu, K. Fundamental Structural Units of the Escherichia Coli Nucleoid Revealed by Atomic Force Microscopy. Nucleic Acids Research 2004, *32* (6), 1982–1992. https://doi.org/10.1093/nar/gkh512.
29. Wolf, S. G.; Frenkiel, D.; Arad, T.; Finkel, S. E.; Kolter, R.; Minsky, A. DNA Protection by Stress-Induced Biocrystallization. Nature 1999, *400* (6739), 83–85. https://doi.org/10.1038/21918.
30. Janissen, R.; Arens, M. M. A.; Vtyurina, N. N.; Rivai, Z.; Sunday, N. D.; Eslami-Mossallam, B.; Gritsenko, A. A.; Laan, L.; de Ridder, D.; Artsimovitch, I.; Dekker, N. H.; Abbondanzieri, E. A.; Meyer, A. S. Global DNA Compaction in Stationary-Phase Bacteria Does Not Affect Transcription. Cell 2018, *174* (5), 1188–1199.e14. https://doi.org/10.1016/j.cell.2018.06.049.
31. Medina, G.; Juárez, K.; Valderrama, B.; Soberón-Chávez, G. Mechanism of Pseudomonas Aeruginosa RhlR Transcriptional Regulation of the RhlAB Promoter. Journal of Bacteriology 2003, *185* (20),

5976–5983. https://doi.org/10.1128/JB.185.20.5976-5983.2003.

32. Young, J. W.; Locke, J. C. W.; Altinok, A.; Rosenfeld, N.; Bacarian, T.; Swain, P. S.; Mjolsness, E.; Elowitz, M. B. Measuring Single-Cell Gene Expression Dynamics in Bacteria Using Fluorescence Time-Lapse Microscopy. Nat Protoc 2012, *7* (1), 80–88. https://doi.org/10.1038/nprot.2011.432.

Figures

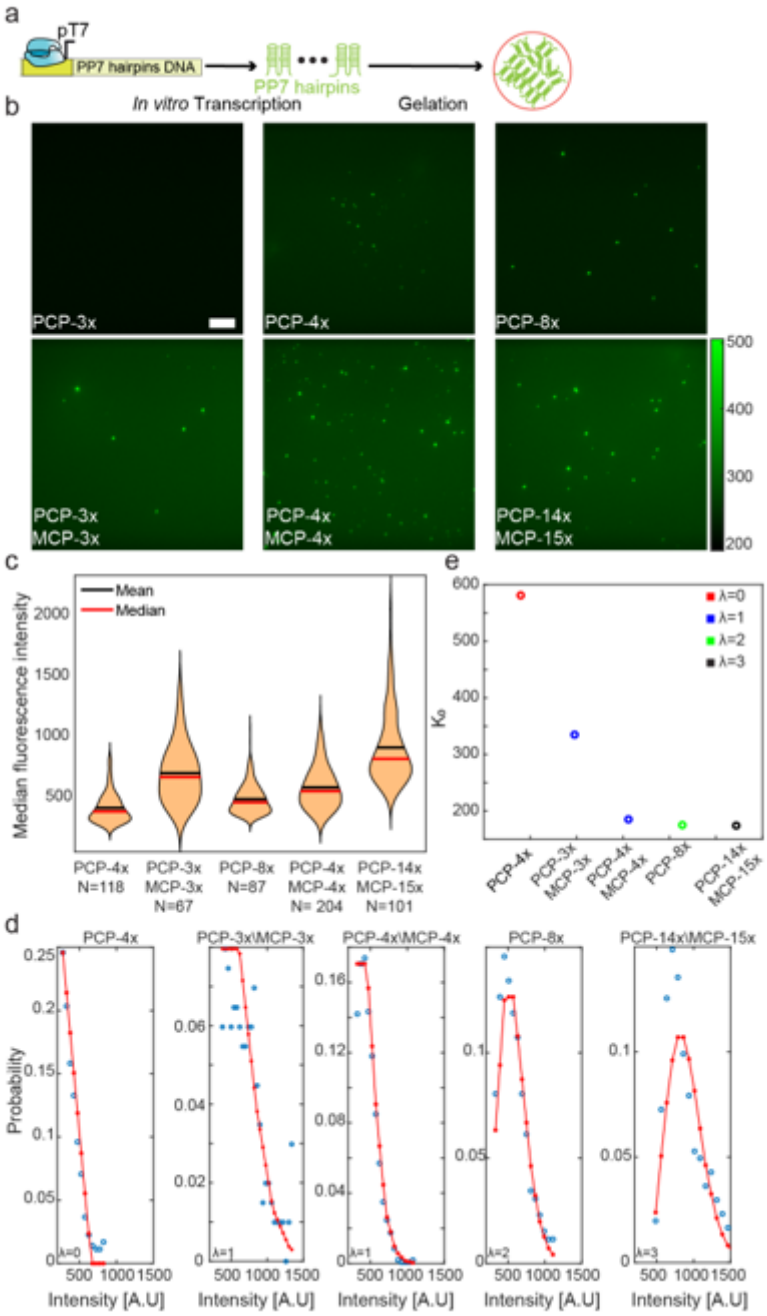

Figure 1

Hairpin-containing slncRNA molecules phase separates *in vitro*. a, Construct diagram depicting *in vitro* transcription of hairpin containing slncRNA molecules used and their gelation under suitable conditions. **b,** Microscopy images showing dependence of structure morphology on the number of binding sites in the slncRNA. PP7-3x results in no visible puncta, while other slncRNAs shows multiple isolated puncta and additional larger fluorescent structures. **c,** Violin plots of median condensate fluorescence of slncRNA-only condensates. **d,** Poisson function fits for the median fluorescence intensities of the slncRNA granules. **e,** K_0 estimates calculated from the Poisson fits, showing a dependence on the number of binding sites in the slncRNA molecule.

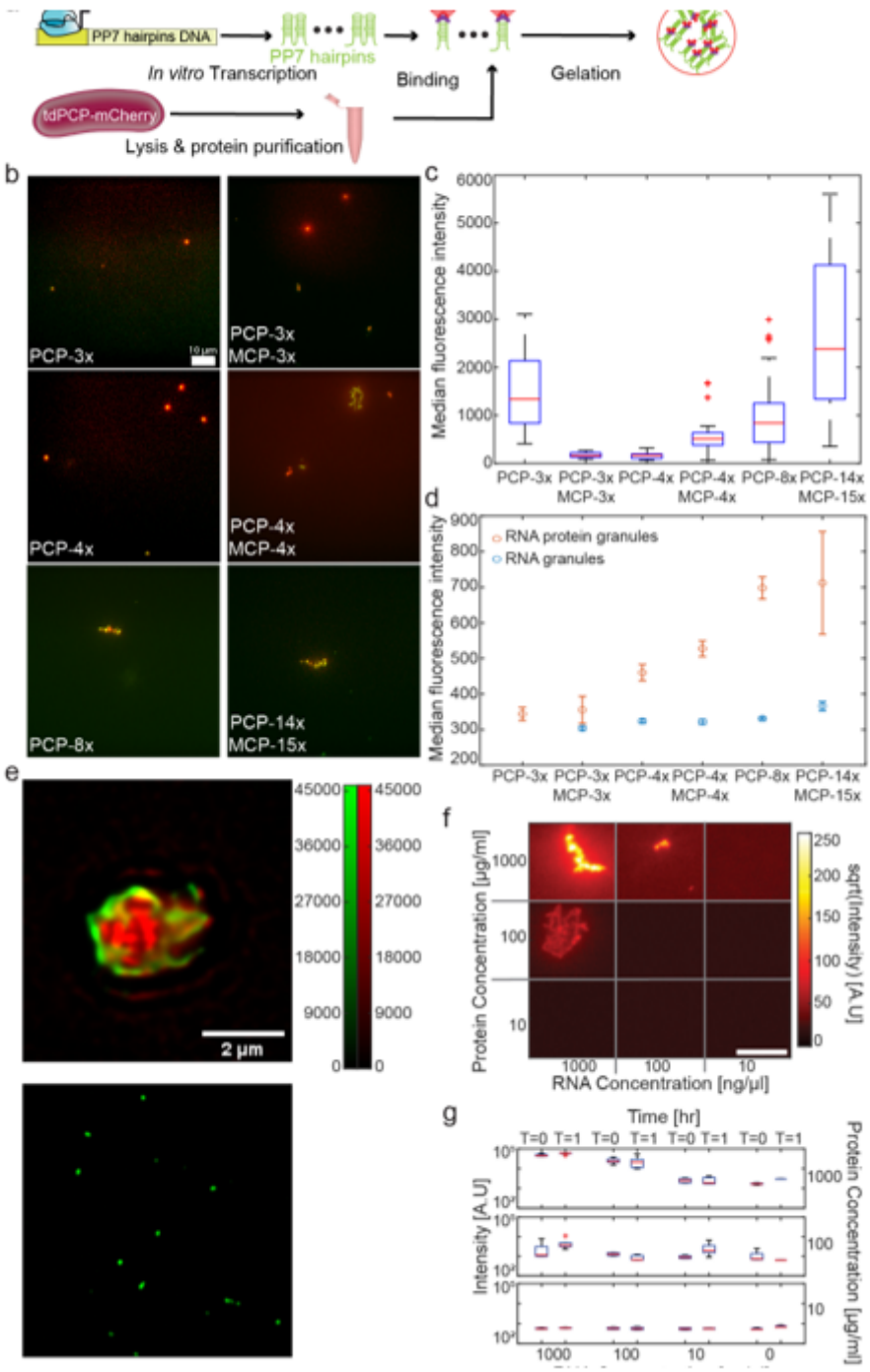

Figure 2

slncRNAs and proteins can form RNA-protein granules *in vitro*. a, Construct diagram depicting the suspension of tdPCP-mCherry recombinant protein together with *in vitro* transcribed slncRNA, resulting in synthetic RNA-protein granules. **b,** Microscopy images showing an overlay of the 585 nm channel (red) and the 488 nm channel (green). **c,** Boxplots of median 585 nm (mCherry) fluorescence intensity values collected from multiple granules. **d**, Mean of median 488 nm (Atto488) fluorescence intensity values collected from multiple slncRNA granules (blue) and slncRNA-protein granules (orange). RNA-protein granule data in panels c,d was collected from 60 PCP-3x granules, 27 PCP-3x/MCP-3x granules, 26 PCP-

4x granules, 31 PCP-4x/MCP-4x granules, 79 PCP-8x granules, and 79 PCP-14x/MCP-14x granules. RNA granule data was collected from 112 PCP-3x/MCP-3x granules, 165 PCP-4x granules, 204 PCP-4x/MCP-4x granules, 121 PCP-8x granules, and 89 PCP-14x/MCP-15x granules. **e,** Structured illumination super resolution images of (Top) slncRNA-protein granule, and (bottom) slncRNA-only granule. Both based on PCP-14x\MCP-15x slncRNA. Scale bar is 2 μm. **f,** Microscopy images for serial dilutions of reaction components taken at T = 1 hr after reaction setup. Highest concentrations show the formation of highly fluorescent filamentous structures, as seen in the top left image. Lower RNA concentrations result in smaller structures, while lower protein concentration result in weaker fluorescence. Scale bar is 10 μm. Due to high dynamic range, the intensities presented are the square root of the raw data images. **g,** Maximal observed intensity values for each reaction condition at time T=0 and T=1 hr.

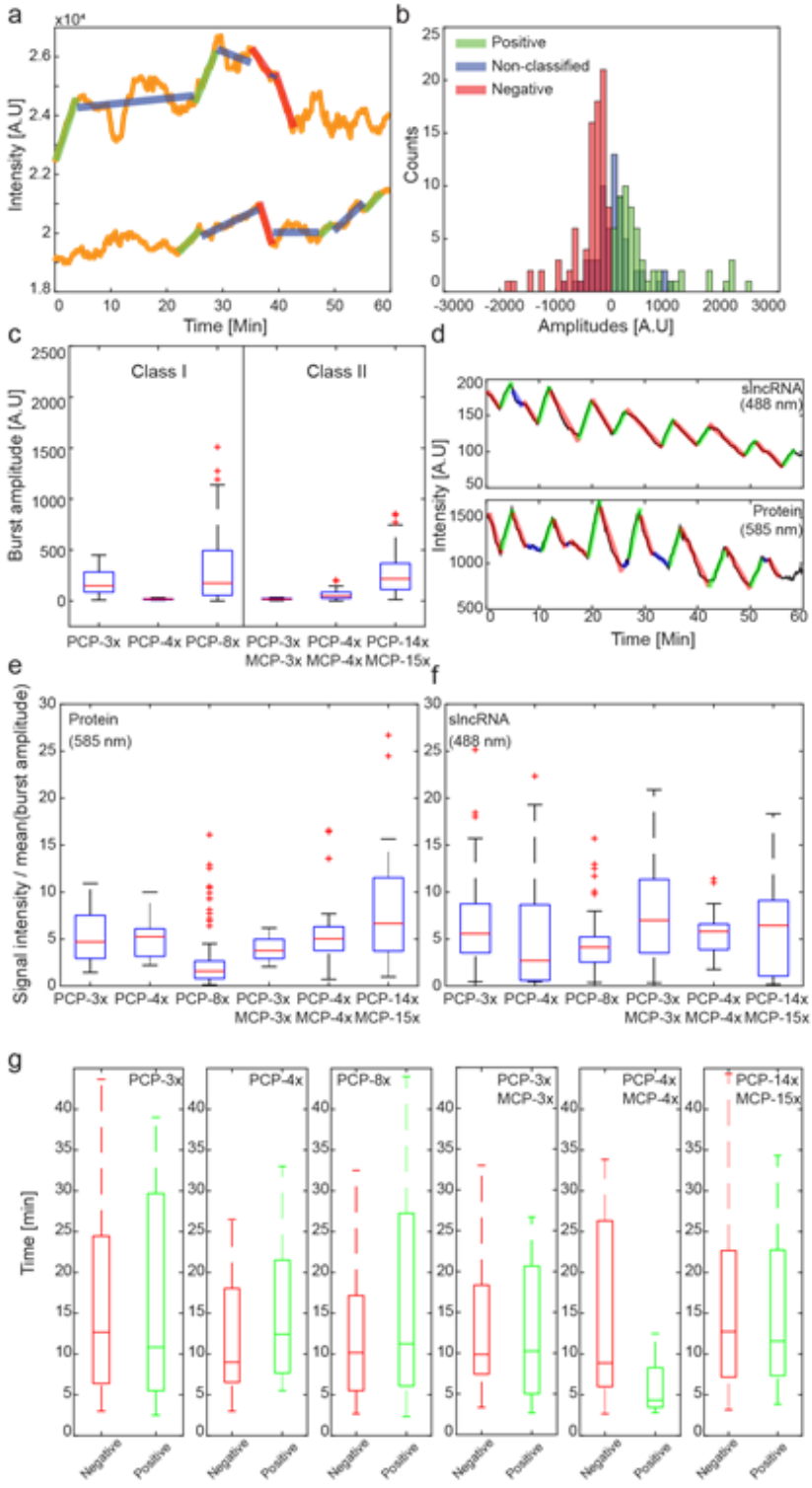

Figure 3

Granule temporal dynamics are dependent on sIncRNA configuration. a, Sample traces of the PCP-14x/MCP-15x sIncRNA with tdPCP-mCherry SRNP granules with annotations of puncta signal. Annotations represent increasing intensity burst events (green), decreasing intensity burst events (red), and non-classified signal (blue), respectively. **b,** Amplitude distributions gathered from ~156 signal traces *in vitro* **c,** Boxplots depicting positive amplitude distributions for all sIncRNAs. **d,** Matching sample traces

of both slncRNA fluorescence (top) and protein fluorescence (bottom) measured from a single granule over the course of 60 minutes. **e,** Boxplots depicting ratio between granule protein fluorescence and mean burst amplitude. **f,** Boxplots depicting ratio between granule slncRNA fluorescence and mean burst amplitude. **g,** Boxplots depicting distributions of durations between a positive burst and a subsequent positive burst (green), and durations between a negative burst and a subsequent negative burst (red). Data in panels c, e, f, g gathered from: 167 traces from PP7-3x granules, 117 traces from PP7-4x granules, 151 traces from PP7-8x granules, 71 traces from PCP-3x/MCP-3x granules, 99 traces from PCP-4x/MCP-4x granules, and 156 traces from PCP-14x/MCP-15x granules.

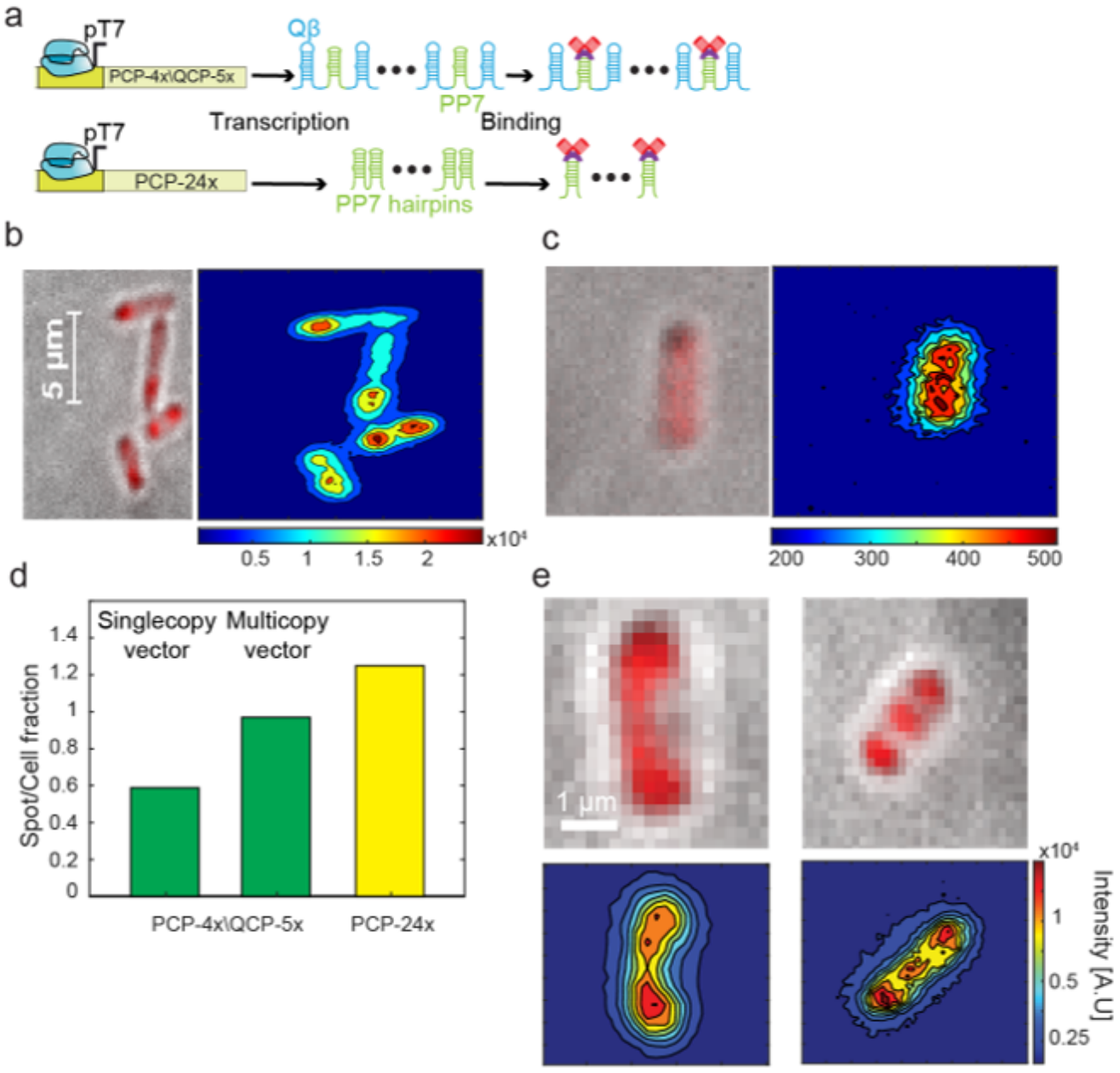

Figure 4

Synthetic phase separated droplets within bacterial cells. a, Construct diagram depicting expression of the two slncRNA cassettes used in the *in vivo* experiments, in the presence of tdPCP-mCherry. **b,** (Left) Merged DIC-585 nm image of cell expressing the PCP-24x slncRNA together with tdPCP-mCherry. (Right) Heatmap of the same image showing a highly fluorescent punctum as the cell pole. Color bar indicates fluorescence intensity. **c,** (Left) Merged DIC-585 nm image of cell expressing the negative control RNA together with tdPCP-mCherry. (Right) Heatmap of the same image showing a weak uniform fluorescence across the cell, color bar indicates fluorescence intensity **d,** Bar plot showing fraction of puncta per cell. (Green) PCP-4x/QCP-5x expressed from either a single copy or a multicopy expression vector. (Yellow) PCP-24x expressed from a single copy vector. **e,** Typical images of fluorescent bacteria in stationary phase, which are different than the 1-2 puncta image obtained for exponentially growing cells. A close examination shows “bridging” or spreading of puncta (left), and emergence of an additional punctum in the middle of the cell (right). Bottom images show heatmaps of the top images.

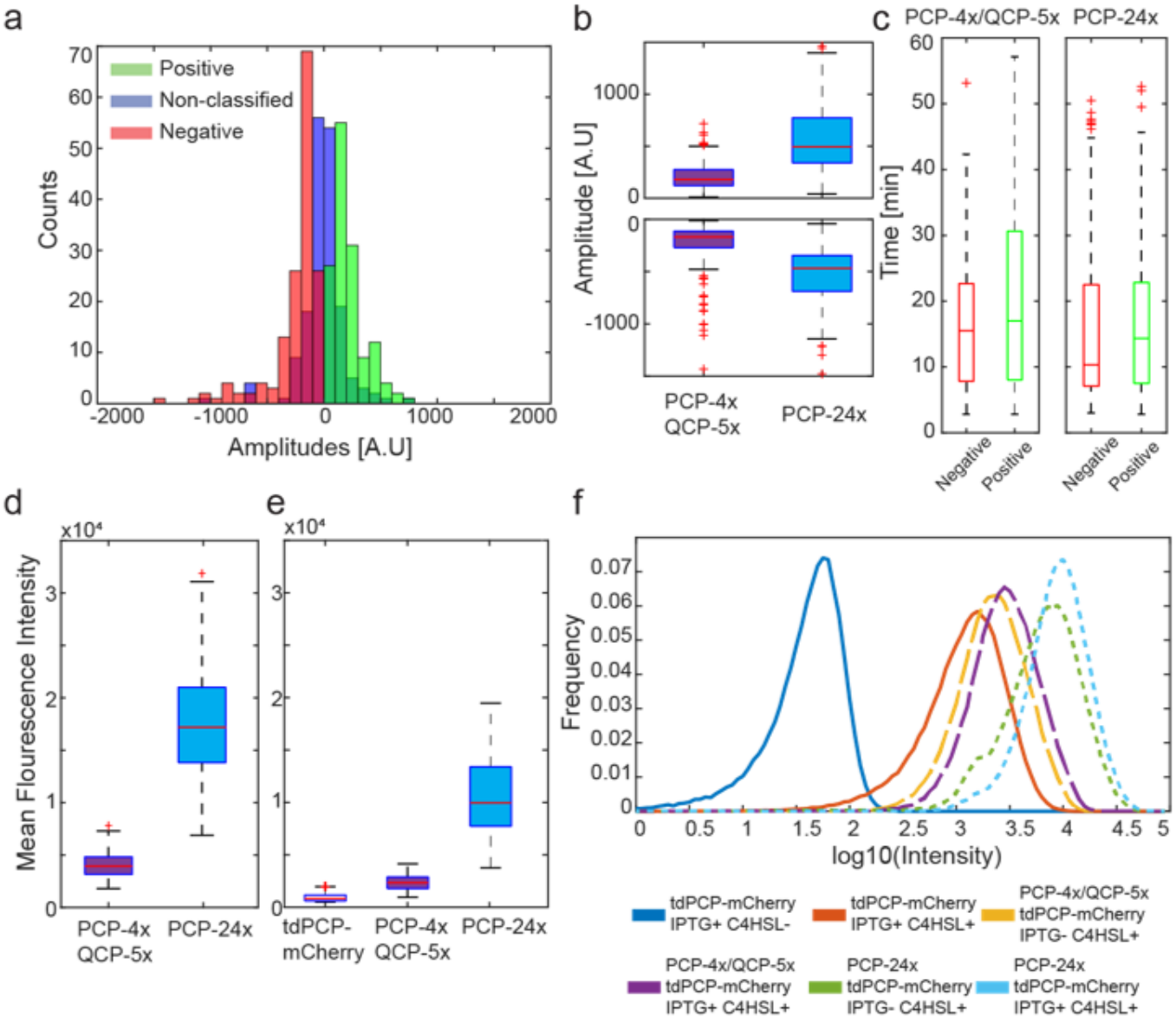

Figure 5

***In vivo* granules present similar dynamics as *in vitro*.** **a,** Empirical amplitude distributions gathered from 255 traces *in vivo* from cells expressing the PCP-4x/QCP-5x slncRNA together with the tdPCP-mCherry protein **b,** Boxplots depicting burst amplitude distributions (top – positive bursts, bottom – negative bursts). **c,** Boxplots depicting distributions of durations between a positive burst and a subsequent positive burst (green), and durations between a negative burst and a subsequent negative burst (red). Data in panels b, c gathered from 255 traces from PCP-4x/QCP-5x granules, and 391 traces from PCP-24x granules. **d,** Boxplot of mean granule fluorescence intensity gathered from 96 PCP-4x/QCP-5x granules, and 182 PCP-24x granules. **e,** Boxplot of mean cell fluorescence intensity. **f,** Population intensities of *E. coli* BL21 cells expressing tdPCP-mCherry with different slncRNAs and different combinations of induction.

Supplementary Files

This is a list of supplementary files associated with this preprint. Click to download.

- RNAgelssupplementaryinformation.docx